The middle Eocene climatic optimum (MECO) event in the Contessa Highway section, Umbrian Apennines, Italy

Luigi Jovane (1, 6), Fabio Florindo (1), Rodolfo Coccioni (2), Jaume Dinarès-Turell (1), Andrea Marsili (2), Simonetta Monechi (3), Andrew P. Roberts (4), Mario Sprovieri (5)

(1) Istituto Nazionale di Geofisica e Vulcanologia, Via di Vigna Murata 605, 00143, Rome, Italy

(2) Istituto di Geologia e Centro di Geobiologia, Università degli Studi di Urbino "Carlo Bo", Campus Scientifico Località Crocicchia, 61029 Urbino, Italy

(3) Dipartimento di Scienze della Terra, Università degli Studi di Firenze, Via La Pira 4, 50121, Florence, Italy

(4) National Oceanography Centre, Southampton, University of Southampton, European Way, Southampton SO14 3ZH, UK

(5) Istituto Ambiente Marino Costiero (CNR), Calata Porta di Massa (Interno Porto di Napoli), 80133, Naples, Italy

(6) Università di Bologna, Dipartimento di Fisica, Via Berti Pichat 8, 40127, Bologna, Italy

Abstract. We report a high-resolution paleomagnetic investigation constrained by new qualitative and semi-quantitative analyses of planktic and benthic foraminifera, nannofossil assemblages, integrated with oxygen and carbon isotope measurements, for the middle Eocene Scaglia limestones of the Contessa Highway section, central Italy. Calcareous plankton assemblages enables recognition of several biostratigraphic events from planktic foraminiferal Zone P11 to the lower part of Zone P15 and from calcareous nannofossil Zone NP15 to the upper part of Zone NP17, which results in refinement of the magnetobiostratigraphy of the Contessa Highway section. Correlation of the paleomagnetic polarity pattern with the geomagnetic polarity timescale provides a direct age interpretation for strata around the middle Eocene Scaglia limestones of the Contessa

Highway section, from Chrons C21n (47 Ma) through to Subchron C18n.1n (38.5 Ma). Bulk carbon isotope values indicate a distinct carbon isotopic shift at 40 Ma that is interpreted to represent the first evidence in the northern hemisphere of the middle Eocene climatic optimum that has recently been observed as a stable isotope anomaly in multiple records from the Indian-Atlantic sector of the Southern Ocean. This should demonstrate a global response of carbon cycle to the proposed transient increased pCO_2 levels during the late middle Eocene and a consequent global CO_2-driven climate change.

Keywords: Eocene, middle Eocene climatic optimum (MECO), magnetostratigraphy, Contessa Highway section, Italy

Introduction

Deep-sea stable isotope records indicate a general high-latitude cooling trend over the last 50 million years (from the early Eocene climatic optimum or EECO), which is thought to have resulted from a combination of factors that altered the amount and distribution of solar radiation over the Earth's surface (e.g., Shackleton and Kennett, 1975; Miller et al., 1991; Zachos et al., 2001; Lear et al., 2004). The *c*. 4‰ increasing trend in $\delta^{18}O$ is not monotonic, but is complex and comprises a series of significant short-term cooling and warming phases, ranging in temporal extent from 10^3 to 10^5 years (e.g., the Oi-1 event in the earliest Oligocene at 34 Ma and the Mi-1 event in the earliest Miocene at 23 Ma; Miller et al., 1991). These signals are superimposed on a long-term trend toward progressively cooler conditions since 50 Ma.

Recently, a distinct negative shift in $\delta^{18}O$ values at 41.5 Ma (designated as the middle Eocene climatic optimum; hereafter, MECO) has been observed in cores from the Indian and Atlantic sectors of the Southern Ocean and is interpreted primarily as a temperature signal that affected both surface waters and middle bathyal deep waters (Bohaty and Zachos, 2003). This peak warming is not mirrored by a significant negative $\delta^{13}C$ excursion, as observed during the

Paleocene-Eocene thermal maximum, which suggests that the MECO event was not triggered by methane-hydrate dissociation but by a transient rise in pCO_2 levels.

The middle Eocene time interval is well represented in pelagic carbonates of the Italian Scaglia Rossa and Scaglia Variegata formations. The Contessa sections (Gubbio, central Italy) contain a thick and continuous Scaglia sequence that extends from the Lower Cretaceous through to the Upper Miocene (e.g., Lowrie et al., 1982; Cresta et al., 1989; Montanari et al., 1997). The middle and upper Eocene Scaglia limestones that crop out along the Contessa Highway (CH) section, have been paleomagnetically investigated by Lowrie et al. (1982). In the same stratigraphic interval that we describe in this paper, Lowrie et al. (1982) collected samples with an average stratigraphic spacing of about 80 cm. They stated that: "the chosen sample spacing was too wide to describe the shorter magnetozones completely" (see also Figure 3 of Lowrie et al., 1982). A higher resolution paleomagnetic reinvestigation was implicitly suggested by this statement. In order to: (1) improve the magnetostratigraphic resolution of the late middle Eocene interval, (2) provide a calibration of biostratigraphic datums in the same interval, and (3) test whether a signature associated with the MECO event is present in this northern hemisphere sequence, which might suggest a global extent for the MECO event, we have developed a new magneto-biostratigraphy, which we integrate with new oxygen and carbon isotope measurements, for the middle Eocene Scaglia limestones of the CH section. This study was carried out within the framework of the "Paleogene Integrated Stratigraphy" (PALIS) project established and sponsored by the Centro di Geobiologia of the University of Urbino.

Location and Geological Setting

The CH section (lat. 43° 22'47" N; long. 13° 33'49" E) is located in the Umbrian region (northeastern Apennines), a few kilometers northwest of Gubbio, which is one of the most ancient towns of Umbria (Figure 1). In this region, depositional environments evolved from a Triassic-Liassic carbonate shelf setting on the continental margin of an African plate promontory, or "Adria"

(Channell et al., 1979), located on the southern margin of the Tethys Ocean, in a pelagic setting (lower to upper bathyal environments) that extended into the Paleogene. The investigated section is fresh and is continuously exposed along a road cut (along Highway 452, "the Contessa Road"). It is about 200 m thick, and extends from the Cretaceous-Tertiary (K-T) boundary through to the Upper Oligocene and consists of the upper part of the Scaglia Rossa (early Turonian to middle Eocene), the Scaglia Variegata (middle Eocene to late Eocene), and the Scaglia Cinerea (late Eocene to Oligocene) (e.g., Cresta et al., 1989). The Paleogene portion of the Scaglia Rossa is made up of 82 m of well-stratified red to pinkish limestones and marly limestones. From 50 to 88 m above the K-T boundary, chert nodules are associated with the limestones ("upper cherty member" of Lowrie et al. (1982)). During the middle Eocene, the amount of clay increased and the Scaglia Rossa grades into about 80 m of gray, green and red bedded marly limestones and calcareous marls of the Scaglia Variegata formation, which has been the focus of this study. The boundary between the Scaglia Rossa and the Scaglia Variegata formations is conventionally placed at 88 m above the K-T boundary, which coincides with the uppermost cherty limestone horizon. In agreement with Monaco et al. (1987), the top of the Scaglia Variegata (upper late Eocene; not studied here) is conventionally placed at the "upper reddish interval" which marks the passage to the overlying Scaglia Cinerea marls. This formation is characterized by alternating grey marly limestones and grey marls that were deposited throughout the Oligocene.

The Scaglia Variegata formation has clear cyclicity within the CH section, with bundles of limestone-marl couplets that suggest the possibility of orbitally controlled deposition (Figure 2). We identified the clear white marker bed at about 99 m, and, from about 110 to 140 m, the distinctive marker beds (clay horizons) termed K, L, M, N, O, P, and Q, as described by Lowrie et al. (1982). The bedding dips 60° to 72° toward the northeast (azimuth of 40° to 54°). A major fault, not described before, is observed in the upper part of the Scaglia Variegata from 139.50 to 140 m, a few meters above the Q recessed interval. The fault dips north at 40°, and is connected to two splays that dip south at 70°. The fault planes contain both dip-slip and strike-slip slickensides.

Previous paleomagnetic investigation of the "Contessa Highway"

In the previous paleomagnetic investigation of the middle and upper Eocene Scaglia limestones of the CH section (Lowrie et al., 1982), the same stratigraphic interval was studied (i.e., from 90 to 150 m above the K-T boundary), with samples collected at an average spacing of about 80 cm. The remanent magnetizations were measured with a 3-axis ScT cryogenic magnetometer (Goree and Fuller, 1976). Pilot samples, selected at c. 4 m intervals, were used to assess the most suitable demagnetization technique for routine treatment. Based on the demagnetization behavior of the pilot samples, they found that thermal treatment was more effective than stepwise alternating field (AF) demagnetization in isolating the characteristic remanent magnetization (ChRM) component in the Scaglia lithologies. The ChRM was generally well defined above 300°C in the Variegata and above 400°C in the Scaglia Rossa samples. It is noteworthy that a small component of magnetization consistently persisted above 600°C. The magnetic reversal stratigraphy for the interval from 95 to 150 m, integrated with planktic foraminiferal biostratigraphy, was correlated with the geomagnetic reversal sequence corresponding to oceanic magnetic anomalies 17 to 21 (LaBreque et al., 1977). A rock magnetic investigation was also carried out, and, based on coercivity spectrum analysis, Lowrie et al. (1982) provided evidence that the main mineral is magnetite, with a hematite component that is pronounced in dark reddish Paleocene Scaglia samples (not studied here).

Methods

Before sampling, and in order to evaluate possible orbital forcing in the studied strata (in progress), a bed-by-bed lithological log was constructed during several field trips (Figure 2).

Paleomagnetism - sampling

The sampled interval of the Scaglia Variegata formation extends from 95 to 150 m above the base of the section. We collected 192 oriented block samples at 5-30 cm intervals and located them with respect to the black and white markers painted onto the section at 5-m stratigraphic intervals by Lowrie et al. (1982). The sample spacing was designed to be closer at reversal boundaries to enable identification of reversals at the individual bed level. Higher resolution sampling was hampered by the presence of a metallic net that is used to maintain slope stability of the road cut. Each oriented hand sample was cut in the laboratory, generally yielding 2 or more 10 cm^3 cubic samples.

Paleomagnetism - laboratory procedures and analysis

Paleomagnetic analyses were carried out within a magnetically shielded laboratory at the Istituto Nazionale di Geofisica e Vulcanologia (INGV), Rome. Natural and artificial magnetic remanences were measured using a narrow-access pass-through cryogenic magnetometer (2-G Enterprises model 750R) with in-line, AF demagnetization capability. Before routine demagnetization was performed for all samples, pilot samples were analysed to determine the most appropriate demagnetization technique for isolating the ChRM. One sample from each stratigraphic level was AF demagnetized at successive peak fields of 5, 10, 15, 20, 25, 30, 40, 50, 60, 80, and 100 milliTesla (mT). Then, sister samples were thermally demagnetized using a magnetically shielded Pyrex furnace at 100, 200, 300, 330, 360, 400, 450, 500, 550, 600, 650, and 700°C. The low-field magnetic susceptibility (χ) was measured after each heating step to monitor for thermal alteration of the magnetic minerals. Thermal and AF demagnetization data were examined using orthogonal vector component diagrams (Zijderveld, 1967); best-fit lines for the progressive demagnetization data were evaluated by principal component analysis (Kirschvink, 1980).

A range of rock magnetic measurements was used to investigate the magnetic mineralogy throughout the investigated section. The low-field mass-specific magnetic susceptibility (χ) was

measured with a Kappabridge KLY-2 magnetic susceptibility meter. Artificial remanences, including the anhysteretic remanent magnetization (ARM) imparted in a 100 mT alternating field, with a superimposed 0.05 mT DC bias field, the isothermal remanent magnetization (IRM) imparted in a field of 0.9 T and back-field demagnetization of the IRM at 0.1 T and 0.3 T were also measured. These data were used to determine the S-ratio (IRM-0.3T/IRM0.9T) and the HIRM (HIRM= (IRM0.9T+IRM-0.3T)/2). These remanences were measured with the 2-G Enterprises magnetometer.

The temperature dependence of magnetic susceptibility was measured up to 700°C on selected samples using a furnace-equipped Kappabridge KLY-3 magnetic susceptibility meter.

First-order reversal curves (FORCs) were analysed on sediment chip samples, using a Princeton Measurements Corporation MicroMag vibrating sample magnetometer at the National Oceanography Centre (NOC), University of Southampton, U.K. Samples were selected for FORC analysis (Roberts et al., 2000) from the intervals with strongest magnetizations.

Foraminiferal assemblages

One hundred and sixty samples were collected (at 30 cm average intervals) for biostratigraphic and stable isotope analyses. The foraminiferal content was analysed for all samples. Foraminifera were studied in washed residues from soft and hard lithologies. Preparation from soft lithologies included gentle crushing, soaking in a hydrogen peroxide solution (10%), sieving through a 63 μm mesh, and drying at 60°C. Preparation from hard lithologies included gentle crushing, cold acetolysis with acetic acid (80%) following the method of Lirer (2000), sieving through a 63 μm mesh, one to two hours cleaning in an ultrasonic cleaner, and drying at 60°C. The cold acetolysis method enables extraction of generally well identifiable foraminifera even from indurated limestones. This offers the possibility of accurate taxonomic determination and detailed analysis of foraminiferal assemblages.

Nannofossil assemblages

Samples for calcareous nannofossil analysis were prepared as smear slides using standard techniques (Bown and Young, 1998). Nannofossils were examined with a light microscope at a magnification of 1000X and were identified following the taxonomic schemes of Perch-Nielsen (1985) and Varol (1998). Assemblages were studied semi-quantitatively, and at least three traverses were investigated for each smear-slide.

Oxygen and carbon isotope measurements

A total of 134 stable isotope analyses were carried out on bulk samples. They were made using an automated continuous flow carbonate preparation GasBenchII device (Spötl and Vennemann, 2003) and a ThermoElectron Delta Plus XP mass spectrometer at the IAMC-CNR (Naples) isotope geochemistry laboratory. Acidification of samples was performed at 50°C. An internal standard (Carrara Marble with $\delta^{18}O$ = -2.43 vs. VPDB and $\delta^{13}C$ = 2.43 vs. VPDB) was run for every 6 samples, and, for every 30 samples, the NBS19 international standard was measured. Standard deviations of carbon and oxygen isotope measurements were estimated at 0.1 and 0.08‰, respectively, on the basis of replicate measurements of ~70 samples. The entire calibration is based directly on standard materials that are part of each run (in our case the homogeneous and certified Carrara Marble carbonate with isotopic composition determined by conventional offline dual-inlet techniques), rather than solving fractionation equations for the acid-based reaction. In other words, there is no need to know the stable isotopic composition of the CO_2 reference gas *a priori*, nor the acid fractionation factor at the given temperature of the reaction (Spötl and Vennemann, 2003). All of the stable isotope data are reported in per mil (‰) relative to the VPDB standard.

Results

Paleomagnetic behavior and polarity zonation

NRM intensities are generally low (Figure 3), especially in the uppermost 10 m of the studied interval (i.e., above 140 m), although there are significant fluctuations (NRM ranges from 6.6 x 10^{-9} Am^2/kg to 1.1 x 10^{-5} Am^2/kg; mean = 2.4 x 10^{-7} Am^2/kg). Intervals with weak magnetizations have more complex behavior during demagnetization (Figure 4). Based on the observed demagnetization behavior, thermal treatment was more effective than stepwise AF demagnetization in removing secondary components and in isolating the ChRM component for both normal and reversed polarity samples (see also Lowrie et al., 1982). Stable paleomagnetic behavior is evident from 92% of the thermally demagnetized samples and from 58% of the AF demagnetized samples. In particular, AF treatment was not effective in removing secondary magnetization components from red-colored intervals.

The magnetic polarity record of the studied portion of the CH section can be subdivided into 7 magnetozones, where the magnetozones are defined as intervals with multiple, consecutive samples with polarities that are distinctly different from neighboring intervals (Figure 5). In a few cases (e.g., 96.90 m, 103.30 m and 133.95 m), isolated samples have polarities opposite to those of the rest of the magnetozone. These samples are not considered in the overall polarity zonation.

Starting from the bottom, the lower 1.08 m of the magnetic polarity record has 3 samples with stable normal polarity (magnetozone N1); the lower boundary of this magnetozone was not sampled. Above magnetozone N1, a predominantly reversed polarity magnetozone dominates from 96.08 m to 110.39 m (magnetozone R1). There is a normal polarity interval from 110.39 and 119.80 m (magnetozone N2) followed by a well-defined reversed polarity interval (magnetozone R2) from 119.80 to 127.45 m. Magnetozone R2 is separated from the overlying reversed polarity interval R3 (from 128.63 to 135.29 m) by a thin (1.21 m thick), but clearly defined, normal polarity interval (N3) that extends from 127.42 to 128.63 m. The uppermost 12.71 m of the studied sequence is dominated by normal polarity (>135.29 m; magnetozone N4). In this magnetozone, 2 samples (at

140.45 and 140.60 m) have reverse polarity. The presence of the aforementioned fault zone contributes to interpretational difficulties in this thin interval (see below).

Rock magnetic properties

Demagnetization behavior, coercivity parameters (S-ratio, HIRM), FORC diagrams, and thermomagnetic analyses all indicate that the magnetic mineral assemblage is dominated by a complex mixture of magnetic minerals that includes magnetite (dominant), maghemite, and hematite (Figures 6-8). For example, the presence of magnetite is indicated in some intervals by S-ratios with values close to unity (Figure 6), marked thermal unblocking at 580°C (Figure 7), and a peak near the origin of the FORC diagram (Figure 8). On the other hand, the presence of hematite is indicated by low S-ratios, high values of HIRM (Figure 6), marked thermal unblocking at 680°C (Figure 7) and a small peak of the FORC distribution at high coercivities of >200-250 mT (Figure 8). Marked decreases in susceptibility were observed after heating to 250-300°C during thermal demagnetization, especially in the reddish intervals (e.g., Figure 4e, o), which we attribute to the presence of maghemite (thermally induced conversion from maghemite to hematite; Stacey and Banerjee, 1974). The abrupt increase in magnetic susceptibility above 400-450°C for most samples (Figure 4) is attributed to thermally induced growth of new magnetite due to the breakdown of smectite during thermal demagnetization (smectite is the dominant clay mineral in the Scaglia Variegata formation (Guerrera et al., 1988; Mattias et al., 1989)).

Interpretation of standard magnetic parameters is complicated in the presence of variable mixtures of magnetic minerals. Regardless, some clear patterns are evident. Only above 140.5 m and at 126-127 m and 116.50-120 m is magnetite the dominant magnetic mineral, without evidence of relatively high coercivity minerals such as hematite (indicated by S-ratios in Figure 6). On the other hand, as would be expected, the stratigraphic intervals with stronger red colorations (95-111 m and 135-139 m) contain significant concentrations of hematite, as indicated by higher HIRM values and lower S-ratios (Figure 6). It should be noted that the boundary between the uppermost

magnetite-dominated interval and the thick underlying interval with a complex mixture of magnetic minerals corresponds to the fault zone at 139.5-140 m (Figure 6**)**. This evidence suggests that a portion of the record could be missing at the fault.

Foraminiferal assemblages

Foraminifera are continuously present, abundant, and diverse throughout the studied section. Preservation varies from poor to good, but is mostly moderate. Paleocene-lower Eocene specimens are occasionally present. The CH section has been previously correlated to the Paleogene planktonic foraminiferal zonation by Lowrie et al. (1982), following the zonal schemes of Bolli (1957a,b, 1966), Blow (1969, 1979), and Premoli Silva and Bolli (1973). Additional biostratigraphic data are also given by Verducci and Nocchi (2004) following Premoli Silva et al. (2003) and in agreement with the criteria used by Pearson and Chaisson (1997).

All of the marker species that define the standard planktonic foraminiferal zones of Berggren et al. (1995) through most of the middle Eocene occur in the analysed material. The lower part of the studied section contains *Morozovella aragonensis* and belongs to the P11 Zone (*Globigerapsis kugleri*/*Morozovella aragonensis* Concurrent Range Zone). The last occurrence (LO) of this species, which defines the P11/P12 (*Morozovella lehneri* Partial Range Zone) zonal boundary, occurs at 112.50 m (Figure 9). The first occurrence (FO) and the LO of *Orbulinoides beckmanni,* which mark, respectively, the P12/P13 (*Globigerapsis beckmanni* Total Range Zone) and the P13/P14 (*Truncorotaloides rohri-Morozovella spinulosa* Partial Range Zone) zonal boundaries, are documented at 135 m and 137 m, respectively (Figure 9).

The LO of large acarinids occurs at 144 m (Figure 9). The LO of *Morozovella spinulosa,* which is the last representative of the *Morozovella* genus, is recognizable at 146 m, where *Truncorotaloides rohri* also disappears. The FO of *Globigerinatheka semiinvoluta* is recorded at 148 m and defines the P14/P15 (*Porticulasphaera semiinvoluta* Interval Zone) zone boundary.

Paleobathymetric assessment is based on the distribution of index forms as reported by Van Morkhoven et al. (1986). The lack of faunal components typical of abyssal depths provides a lower depth limit of 2000 m. The high abundance of *Cibicidoides eocaenus*, *C. mexicanus*, *Globocassidulina subglobosa*, *Hanzawaia ammophila*, *Nuttallides truempyi*, and *Planulina costata,* together with some specimens of *Aragonia aragonensis,* indicates a middle-lower bathyal setting (800-1000 m). Although some of the bathymetric indicators fluctuate in relative abundance or even locally disappear, no remarkable paleobathymetric change is evident throughout the studied section. Accordingly, the P/P+B x 100% (P = planktic; B = benthic) ratio has constant values that are typical of bathyal depositional environments.

Nannofossil assemblages

Calcareous nannofossils are abundant throughout the studied interval even if they are not well preserved and have low diversity. Most of the important markers used to define the standard zonations of Martini (1971) and Okada and Bukry (1980) are recognised. Several additional marker species are also documented here.

Monechi and Thierstein (1985) reported biostratigraphic results from the Eocene interval of the CH section using the CP zones of Okada and Bukry (1980). Our re-examination of the interval allows recognition of several important and well-known markers, such as the LO of *Chiasmolithus gigas* (CP13b Subzone). *Chiasmolithus* is not common in the Scaglia formation owing to paleoecological and preservation problems; low relative abundances have led to discontinuous occurrences. Regardless, FO and LO determinations are moderately reliable. While a few specimens of *Reticulofenestra umbilica* > 14 μm are present above 119 m, we define its first common occurrence (FCO) at 122 m, together with the LO of *Nannotetrina* spp (Figure 9). A discrepancy between this identification and that of Monechi and Thierstein (1985) is due to the different taxonomic concept of *R. umbilica* size > 12.5 μm in Monechi and Thierstein (1985).

Several additional calcareous nannofossil events can be used to improve the biostratigraphic framework. The FO and LO of *Sphenolithus furcatolithoides*, two events reported by Catanzariti and Perilli (2004) in Eocene formations from the northern Appennines (Italy) are detected in the studied stratigraphic interval (Figure 9). The FO of *Dictyococcites scrippsae* (*D. hesslandii* of Backman, 1987) at 137 m seems to be a distinct event and could approximate the base of Zone CP14b or Zone NP17 (Lyle et al., 2002.), which is marked by the LO of *Chiasmolithus solitus*. A major change in the nannofossil content is marked by the FCO of *Dictyococcites bisectus* > 10 μm at around 145-148 m, which becomes abundant at 148-149 m (Figure 9).

Oxygen and carbon isotopes

Bulk carbon isotope values (Figure 10) range between +1.2 and +2.2‰, which correspond to values for biogenic calcite precipitated under open marine conditions during the Paleocene and Eocene (e.g., Bohaty and Zachos, 2003). On the other hand, $\delta^{18}O$ values (not shown here) range between -3.5 and -0.5‰ and are depleted by ~3‰ relative to diagenetically unaltered marine calcite (Bohaty and Zachos, 2003). We interpret these data to suggest that the oxygen isotopic composition of the measured samples reflects elevated temperature during burial diagenesis and/or the effects of meteoric diagenesis, while the carbon isotopic composition has been less affected by these processes. It is noteworthy that a global significance of the $\delta^{13}C$ signal has been previously inferred in other stratigraphic intervals of the Paleogene in the CH section (e.g., Corfield et al., 1991).

The $\delta^{13}C$ curve contains a long positive excursion that rises from average values of 1.4‰ at the base of the studied section to a maximum of almost 2‰ at 112 m. Higher frequency oscillations of ±0.3‰ about an average $\delta^{13}C$ value of 1.6‰ characterizes the signal above the positive excursion at 112 m. The most notable feature of the $\delta^{13}C$ curve is a positive peak that rises by 0.6‰, starting at 133.5 m and peaking at about 138.5 m. After the peak, the $\delta^{13}C$ values swing back to average values of about 1.6‰ between 138.5 and 139.5 m.

DISCUSSION

Correlation to the geomagnetic polarity time scale

We provide here an interpretation of the magnetic polarity pattern of the middle Eocene Scaglia limestones that crop out in the CH section, constrained by new analyses of planktic foraminifera and calcareous nannofossil assemblages. The geomagnetic polarity time scale (GPTS) used in this study is that of Berggren et al. (1995) and Cande and Kent (1995). Our magnetostratigraphic interpretation for the interval between 95 and 139 m is straightforward and provides a direct correlation with the GPTS between the top of Chron C21n (46.26 Ma) and Chron C18n.2n (39.63-40.13 Ma) (Figure 9). Most of the recorded bioevents fall on or near the correlation line between our magnetic polarity zonation and the GPTS. Of these events, the LO of *Morozovella* spp. and *Truncorotaloides rohri* (P2) do not fall on the magnetostratigraphic correlation line, which might be related to the presence of the fault zone between 139.5 and 140 m. Above 140 m, the FCO of *Dictyococcites bisectus* (N1) and the FO of *Globigerinatheka semiinvoluta* (P1) suggest the possibility that the uppermost portion of magnetozone N4 above the fault zone correlates to Chron C18n.1n. With this interpretation, at mimimum Subchron C18n.1r (39.55-39.63 Ma) is inferred to be missing in the fault zone between 139.5 and 140 m. The average sedimentation rate for the interval between 135.29 m (base of Chron C18n.2n) and 96.08 m (top of Chron C21n) is 6.4 m/m.y. (0.64 cm/k.y). Previous estimates of the sedimentation rate in the Eocene Scaglia Variegata and Scaglia Rossa, as deduced from paleontological dating and the numerical time scale of Hardenbol and Berggren (1978), were of the order of 9 m/m.y. (see Lowrie et al., 1982).

Stable isotopes and the MECO event

On the basis of the above correlation to the GPTS, the distinct ~0.6‰ increase in bulk $\delta^{13}C$ values observed in the middle Eocene of the CH section occurred from the top of Chron C18r through to Subchron C18n.2n at about 40 Ma (Figures 9, 10). The magnitude and duration of the $\delta^{13}C$ shift are comparable to the MECO stable isotope anomaly (positive shift of ~0.6‰ and

duration of ~600 k.y.), which has been observed in multiple records from the Indian-Atlantic sector of the Southern Ocean and is interpreted as an interval of "significant transient warming" (Bohaty and Zachos, 2003). In these records, the age of the MECO event was calculated primarily from nannofossil datums and was placed at 41.5 Ma. At Maud Rise (ODP Sites 689) and Kerguelen Plateau (ODP sites 738 and 748), the event is associated with the FO of the nannofossil *Reticulofenestra reticulata (*ex *Cribrocentrum reticulatum*), which occurs just below the MECO event. The 1.5 m.y. mismatch between the MECO event identified in Southern Ocean deep-sea cores and the stable isotope anomaly identified at the CH section might reflect the uncertain calibration of *R. reticulata* in Southern Ocean sections. Crucially, the Kerguelen Plateau ODP sites do not have a reliable magnetostratigraphy in the vicinity of the MECO event. The original magnetostratigraphic studies of these sites are unreliable, and a recent re-analysis demonstrated that this interval in ODP Hole 748B was weakly and unstably magnetized (Roberts et al., 2003).

Among the Southern Ocean records, Hole 690B probably has the best middle Eocene magnetostratigraphic record, but this part of the section is riddled with hiatuses (Florindo and Roberts, 2005). There, the FO of *R. reticulata* occurs just below a normal polarity interval (see Figures 12 and 13 of Florindo and Roberts, 2005), which was interpreted to correlate with Chron C19n, although it is also possible that this polarity interval could represent the bottom of C18n.2n.

In Hole 1090B (ODP Leg 177), the FO of *R. reticulata* occurs near the C18r/C19n reversal (Marino and Flores, 2002). The quality of the inclination data below ~C17n (~345 mbsf), however, is not good, so this might not be the best site to calibrate this datum. In Hole 1172A (ODP Leg 189), the FO of *R. reticulata* occurs between 414.29 and 417.29 mbsf (Wei et al., 2003), just below the base of C18n.2n at 415 mbsf (Stickley et al., 2004). However, it is worth noting that nannofossils are sparse below ~415 mbsf and this may not therefore represent the "true" FO of *R. reticulata*. Overall, the Southern Ocean data indicate that the age of the MECO event remains poorly calibrated.

Conclusions

New magneto-biostratigraphic results from the middle Eocene Scaglia limestones of the Contessa Highway section can be directly correlated to the GPTS from Chron C21n through to Subchron C18n.1n, which corresponds to the time interval between 47 and 38.5 Ma (Berggren et al., 1995). A significant fault zone occurs in the upper part of the CH section, which removed, in our interpretation, at least Subchron C18n.1r.

Bulk carbon isotope values indicate a distinct increase in bulk $\delta^{13}C$ values at the top of Chron C18r through to Subchron C18n.2n at about 40 Ma. This carbon shift is comparable in magnitude and duration to the MECO stable isotope anomaly recently observed in multiple records from the Indian-Atlantic sector of the Southern Ocean that is dated at about 41.5 Ma (Bohaty and Zachos, 2003).

It is noteworthy that just following the observed stable isotope anomaly (i.e., the MECO event) a significant biotic turnover in planktonic foraminifera takes place with a notable reduction in the acarinid lineage and the extinction of the morozovellids and other muricate species. This would suggest connected causal mechanisms between these events.

Our data from the CH section provide the first evidence of the MECO event beyond the Southern Ocean, which suggests a global response of the oceanic carbon cycle to the same forcing that is not confined to the Indian and Atlantic sector of the Southern Ocean. We suggest that the ~1.5 m.y. mismatch might reflect significant uncertainty in the calibration of *R. reticulata* in Southern Ocean sedimentary sequences.

Finally, high-frequency rhythms have been recognized in our new bed-by-bed lithological profile of the Scaglia Variegata formation (with variable bundling of marly limestone-marl couplets). Spectral analysis techniques are under detailed investigation to search for periodicities to determine whether these cycles were orbitally controlled.

References

Backman, J., 1987, Quantitative calcareous nannofossil biochronology of middle Eocene through early Oligocene sediments from DSDP Site 522 and 523: Abhandlungen der Geologische Bundesanstalt, v.39, p. 21-31.

Berggren, W.A., Kent, D.V., Swisher, C.C., Aubry, M.P., 1995, A revised Cenozoic geochronology and chronostratigraphy, *in* Berggren, W.A., Kent, D.V., Aubry, M.P., Hardenbol, J. (Eds.), Geochronology, Time Scales and Global Stratigraphic Correlation, Society for Sedimentary Geology (SEPM) Special Publication 54, p. 129-212.

Blow, W.H., 1969, Late middle Eocene to Recent planktonic foraminiferal biostratigraphy, *in* Brönniman, P., Renz, H.H. (eds.), Proc. 1st International Conference on Planktonic Microfossils (Geneva, 1967). E.J. Brill, Leiden, v. 1, p. 199-421.

Blow, W.H., 1979, The Cenozoic Globigerinida: A Study of the Morphology. Taxonomy. Evolutionary Relationships and the Stratigraphical Distribution of some Globigerinida (mainly Globigerinacea): Leiden, E.J. Brill, v. 3, p. 1413.

Bohaty, S. M., and Zachos, J. C., 2003, Significant Southern Ocean warming event in the late middle Eocene: Geology, v. 31, p. 1017-1020.

Bolli, H.M., 1957a, The genera *Globigerina* and *Globorotalia* in the Paleocene-lower Eocene Lizard Springs Formation of Trinidad: B.W.I., United States National Museum Bulletin, v. 215, p. 51-81.

Bolli, H.M., 1957b, Planktonic foraminifera from the Eocene Navet and San Fernando formations of Trinidad: B.W.I., United States National Museum Bulletin, v. 215, p. 155-172.

Bolli, H.M., 1966, Zonation of Cretaceous to Pliocene marine sediments based on planktonic foraminifera: Boletino Informativo Associacion Venezolana de Geologia, Mineria y Petrolio, v. 9, p. 3-32.

Bown, P.R., and Young, J., 1998, Techniques, *in* Calcareous Nannofossil biostratigraphy, Bown P.R. (ed.) Chapman & Hall, p. 16-28.

Cande, S.C., and Kent, D.V., 1995, Revised calibration of the geomagnetic polarity time scale for the late Cretaceous and Cenozoic: Journal of Geophysical Research, v. 100, p. 6093–6095, doi: 10.1029/94JB03098.

Catanzariti R., and Perilli N., 2004, Nannobiohorizons recognised in Eocene formations from the Northern Appennines (Italy): Ina10 Abstracts, Lisbon. Journal of Nannoplakton Research, v. 26, p. 16-17.

Channell, J.E.T., D'Argenio, B., and Horwath, F., 1979, Adria, the African Promontory, *in* Mesozoic Mediterranean Palaeogeography: Earth Science Review, v. 15, p. 213-292.

Channell, J.E.T., Freeman, R., Heller, F., and Lowrie, W., 1982, Timing of diagenetic haematite growth in red pelagic limestones from Gubbio (Italy): Earth and Planetary Science Letters, v. 58, p. 189-201.

Corfield, R.M., Cartlidge, J.E., Premoli-Silva, I., Housley, R.A., 1991, Oxygen and carbon isotope stratigraphy of the Palaeogene and Cretaceous limestones in the Bottaccione Gorge and the Contessa Highway sections, Umbria, Italy: Terra Nova, v.3, p. 414-422.

Cresta, S., Monechi, S., and Parisi, G., 1989, Stratigrafia del Mesozoico al Cenozoico nell'area Umbro-Marchigiana: Memorie Descrittive della Carta Geologica d'Italia, v. 34, p. 185.

Florindo, F., Roberts, A.P., 2005, Eocene-Oligocene magnetobiochronology of ODP Sites 689 and 690, Maud Rise, Weddell Sea, Antarctica: Geological Society of America Bullettin, v. 117, p. 46-66.

Guerrera, F., Monaco, P., Nocchi, M., Parisi, G., Franchi, R., Vannucci, S., Giovannini, G., 1988, La Scaglia Variegata Eocenica nella sezione di Monte Cagnero (bacino marchigiano interno): studio litostratigrafico, petrografico e biostratigrafico: Bollettino Società Geologica Italiana, v. 107, p. 81-99.

Handerbol, J., and Berggren, W.A., 1978, A new Paleogene numerical time scale, *in* Cohee, G.V., Glaessner, M.F., and Hedberg, H.D., eds., Contributions to the geologic time scale; studies in geology, Tulsa, Oklahoma, American Association of Petroleum Geologists, v. 6, p. 213-234.

Kirschvink, J. L., 1980, The least-squares line and plane and the analysis of paleomagnetic data: Geophysical Journal of the Royal Astronomical Society, v. 62, p. 699– 718.

LaBreque, J.L., Kent, D.V., and Cande, S.C., 1977, Revised magnetic polarità time scale for Late Cretaceous and Cenozoic time: Geology, v. 5, p. 330-335.

Lear, C.H., Rosenthal, Y., Coxall, H.K., Wilson, P.A., 2004, Late Eocene to early Miocene ice sheet dynamics and the global carbon cycle: Paleoceanography, v. 19, PA4015, doi:10.1029/2004PA001039.

Lirer, F., 2000, A new technique for retrieving calcareous microfossils from lithified lime deposits: Micropaleontology, v. 46, p. 365-369.

Lowrie, W., Alvarez, W., Napoleone, G., Perch-Nielsen, K., Premoli Silva, I., Toumarkine, M., 1982, Paleogene magnetic stratigraphy in Umbrian pelagic carbonate rocks: The Contessa sections, Gubbio: Geological Society of America Bulletin, v. 93, p. 414-432.

Lyle, M., Wilson, P.A., Janecek, T.R., et al., 2002, Proc. ODP, Init. Repts., 199 [Online], Available from World Wide Web: http://www-odp.tamu.edu/publications/199_IR/199ir.htm.

Marino, M., and Flores, J. A., 2002, Middle Eocene to Early Oligocene calcareous nannofossil stratigraphy at Leg 177 Site 1090: Marine Micropaleonatology, v. 45, p. 383-398.

Martini, E., 1971, Standard Tertiary and Quaternary calcareous nannoplankton zonation, *in* Farinacci, A., ed., Proceedings of the Second Planktonic Conference, Roma 1970, Tecnoscienza, Roma, v. 2, p. 739-785.

Mattias, P., Farabollini, P., and Montanari, A., 1989, Aspetti minero-petrografici della Scaglia Variegata nella serie pelagica della valle della Contessa, presso Gubbio, Umbria orientale: Studi Geologici Camerti, v. 11, p. 7-14.

Miller, K. G., Wright, J. D., and Fairbanks, R. G., 1991, Unlocking the ice house: Oligocene-Miocene oxygen isotopes, eustacy and margin erosion: Journal of Geophysical Research, v. 96, p. 6829– 6848.

Monaco, P., Nocchi, M., and Parisi, G., 1987, Analisi stratigrafica e sedimentologica di alcune sequenze pelagiche dell'Umbria sud-orientale dall'Eocene inferiore all'Oligocene inferiore: Bollettino Società Geologica Italiana, v. 106, p. 71-91.

Monechi, S., Thierstein, H.R., 1985, Late Cretaceous-Eocene nannofossil and magnetostratigraphic correlations near Gubbio, Italy: Marine Micropaleonatology, v. 9: p. 419-440.

Montanari, A., Bice, D.M., Capo, R., Coccioni, R., Deino, A., De Paolo, D.J., Emmanuel, L., Monechi, S., Renard, M. and Zevenboom, D., 1997, Integrated stratigraphy of the Chattian to mid-Burdigalian pelagic sequence of the Contessa valley (Gubbio, Italy), *in* Montanari, A., Odin, G.S., and Coccioni, R. (Eds), Miocene Stratigraphy: an Integrated Approach, Elsevier Sciences, p. 249-277.

Okada, H., and Bukry, D., 1980, Supplementary modification and introduction of code numbers to the low-latitude coccolith biostratigraphic zonation (Bukry, 1973; 1975): Marine Micropaleontology, v. 5, p. 321-325.

Perch-Nielsen, K., 1985, Mesozoic calcareous nannofossils. *in* Bolli, H.M., Saunders, J.B., Perch-Nielsen, K. (Eds.), Plankton Stratigraphy, Cambridge Univiversity Press, Cambridge, p. 329–426.

Premoli Silva, I., Bolli, H.M., 1973, Late Cretaceous to Eocene planktonic foraminifera and stratigraphy of Leg 15 sites in the Caribbean Sea. *in* Edgar, N.T., Saunders, J.B. et al. (Eds.), Initial Reports of the Deep Sea Drilling Project, v. 15, p. 449-547.

Roberts, A.P., Pike, C.R., Verosub, K.L., 2000, FORC diagrams: a new tool for characterizing the magnetic properties of natural samples: Journal of Geophysical Research, v. 105, p. 28461-28475.

Roberts, A.P., Bicknell, S.J., Byatt, J., Bohaty, S.M., Florindo F., and Harwood, D.M., 2003, Magnetostratigraphic calibration of Southern Ocean diatom datums from the Eocene - Oligocene of Kerguelen Plateau (Ocean Drilling Program sites 744 and 748): Palaeogeography, Palaeoclimatology, Palaeoecology, v. 198, p. 145-168.

Roggenthen, W.M., 1979, Magnetic mineralogy of pelagic limestone, Gubbio, Italy: Transaction of American Geophysical Union, v. 60, p. 246, abstract.

Shackleton, N.J., and Kennett, J.P., 1975, Paleotemperature history of the Cenozoic and the initiation of Antarctic glaciation: Oxygen and carbon isotope analyses in DSDP Sites 277, 279, and 281: Initial Rep. Deep Sea Drill. Project, v. 29, p. 743-755.

Spötl, C., and Vennemann, T.W., 2003, Continuous-flow isotope ratio mass spectrometric analysis of carbonate minerals: Rapid Communications Mass Spectrometry, v. 17, p. 1004-1006.

Stacey, F.D. and Banerjee, S.K., 1974,The Physical Principles of Rock Magnetism, Elsevier, New York.

Stickley, C.E., Brinkhuis, H., McGonigal, K.L., Chaproniere, G.C.H., Fuller, M., Kelly, D.C., Nürnberg, D., Pfuhl, H.A., Schellenberg, S.A., Schoenfeld, J., Suzuki, N., Touchard, Y., Wei, W., Williams, G.L., Lara, J., and Stant, S.A., 2004, Late Cretaceous-Quaternary biomagnetostratigraphy of ODP Sites 1168, 1170, 1171, and 1172, Tasmanian Gateway, *in* Exon, N.F., Kennett, J.P., and Malone, M.J. (Eds.), Proc. ODP, Sci. Results, 189 [Online]. Available from World Wide Web: http://www-odp.tamu.edu/publications/189_SR/111/111.htm.

Van Morkhoven, F.P.C.M., Berggren, W.A., and Edwards, A.S., 1986, Cenozoic Cosmopolitan Deep-Water Benthic Foraminifera: Bulletin Centre Recherces Exploration-Production: Elf-Aquitaine, Memories, v. 11, p.421.

Varol, O., 1998, Paleogene, *in* Bown, P.R. (Ed.), Calcareous Nannofossil Biostratigraphy. Kluwer Academic Publishing, Dordrecht, p. 201-224.

Verducci, M. and Nocchi, M., 2004, Middle to Late Eocene main planktonic foraminiferal events in the Central Mediterranean area (Umbria-Marche basin) related to paleoclimatic changes: Neues Jahrbuch für Geologie und Paläontologie, Abhandlungen, v. 234, p. 361-413.

Wei, W., McGonigal, K.L., and Zhong, S., 2003, Data report: Paleogene calcareous nannofossil biostratigraphy of ODP Leg 189 (Australia-Antarctica Gateway), *in* Exon, N.F., Kennett, J.P.,

and Malone, M.J. (Eds.), Proc. ODP, Sci. Results, 189 [Online]. Available from World Wide Web: http://www-odp.tamu.edu/publications/189_SR/103/103.htm.

Zijderveld, J. D. A., 1967, A.C. demagnetization of rocks: Analysis of results, *in* Methods in Paleomagnetism, edited by D. W. Collinson, Elsevier Sciences., New York, p. 254– 286.

FIGURE CAPTIONS

Figure 1. Schematic geological map of the NW-SE trending Gubbio structure and location of the Contessa sections (CH=Contessa Highway; CQ=Contessa Quarry; CR=Contessa Road) on a simplified map that gives the formation boundaries in the Contessa Valley.

Figure 2. Detailed lithostratigraphic column for the interval between 95 and 151 m for the CH section. Samples collected for this study and colours of the lithologies are also indicated.

Figure 3. Stratigraphic variations of intensity and inclination of the natural remanent magnetization (NRM). A detailed lithostratigraphic column for the interval between 95 and 151 m is shown to the left.

Figure 4. Thermal and AF demagnetization diagrams in tilt corrected coordinates for twenty representative "sister" specimens. Open circles = projection onto the vertical plane; full circles = projection onto the horizontal plane. Best-fit lines are only shown for samples with identifiable ChRM components. Insets: Magnetic susceptibility measurements made after each heating step for thermal demagnetization.

Figure 5. Stratigraphic variations of (a) declination and (b) inclination of the characteristic remanent magnetization (ChRM). The magnetic polarity zonation is shown on the log to the right. Black (white) represents normal (reversed) polarity intervals. (c) Inclination variations of the ChRM for the same sequence from Lowrie et al. (1982).

Figure 6. Stratigraphic variations in magnetic properties for the CH section, including low-field magnetic susceptibility, ARM, IRM, HIRM (=(IRM0.9T+IRM-0.3T)/2), S-ratio (=IRM-0.3T/IRM0.9T). A detailed lithostratigraphic column for the interval between 95 and 151 m is shown to the right. See text for discussion.

Figure 7. Temperature dependence of magnetic susceptibility for six selected samples up to a maximum temperature of 700°C. A clear decrease in susceptibility is evident near 580°C for most of these samples, which indicates the Curie temperature of magnetite. Moreover, some samples (e.g., 121.95 m) also display a broad bump centred at 250°C followed by a marked

decrease in magnetic susceptibility, which can be interpreted in terms of conversion from maghemite to hematite (e.g., Stacey and Banerjee, 1974). Above 600°C the magnetic susceptibility is weak compared to the sensitivity of the instrument, but it is still possible to discern evidence of the Curie temperature of hematite (680°C). The data are corrected for the diamagnetism of the furnace.

Figure 8. Representative FORC diagram (smoothing factor, SF = 9) for a sample from 131.40 m. The dominant peak near the origin is consistent with the presence of magnetite, while the small peak at H_c = 200-250 mT indicates the presence of a high coercivity mineral (e.g., hematite).

Figure 9. Age vs. stratigraphic thickness plot with correlation of the CH section polarity zonation to the geomagnetic polarity time scale (GPTS) of Cande and Kent (1995). Calcareous nannofossil (N) and planktonic foraminiferal (P) datums are used to constrain the interpretation.

Figure 10. Detailed lithostratigraphic column for the interval between 95 and 151 m, along with the magnetostratigraphic interpretation and the carbon isotope record of the Contessa section. Stable isotope data are also shown from ODP Hole 748B between 50 and 32 Ma for comparison of the MECO event (modified from Bohaty and Zachos, 2003).

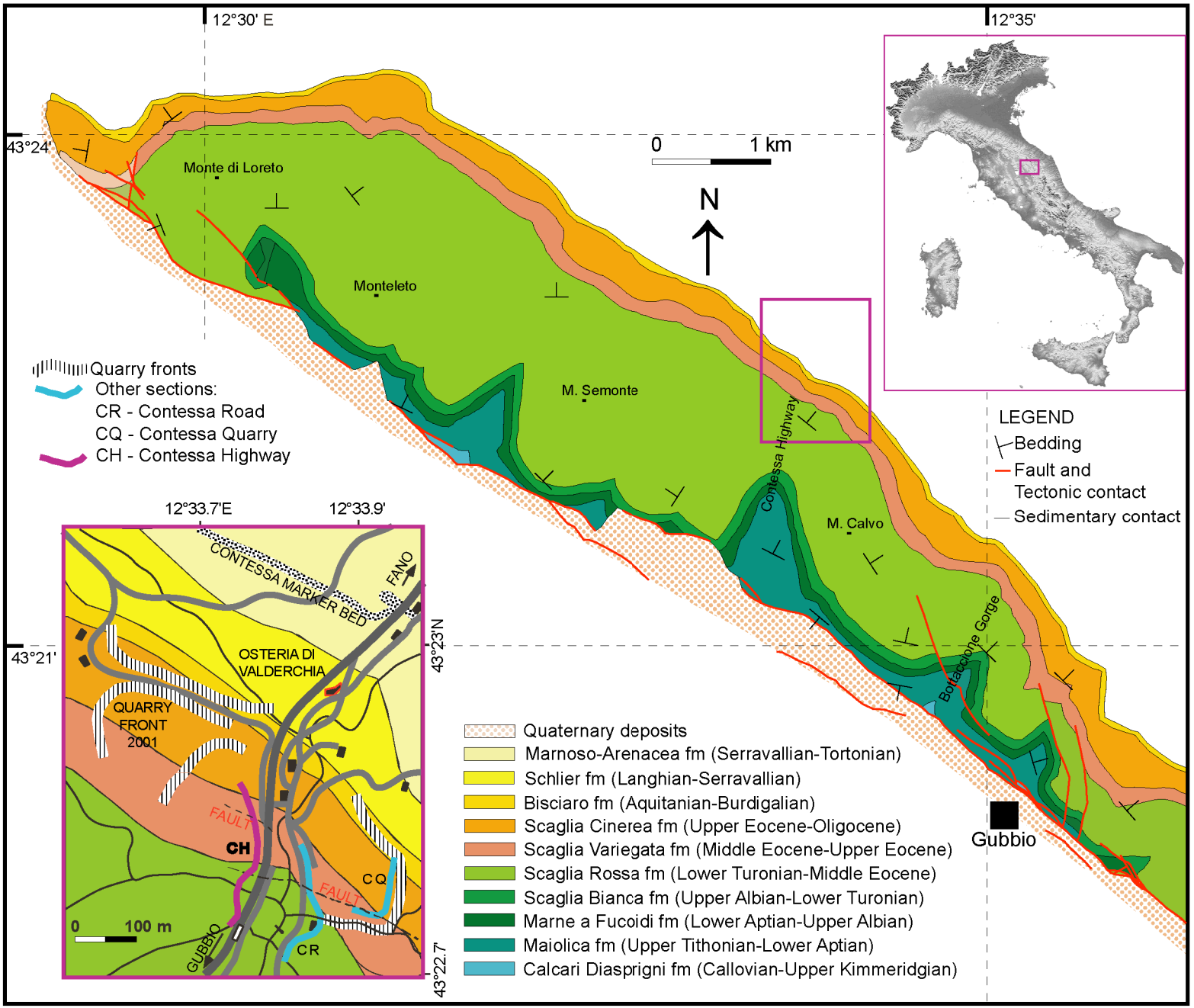
12°30' E
12°35'
43°24'
43°21'
0
1 km
N
Monte di Loreto
Monteleto
M. Semonte
M. Calvo
Contessa Highway
Bottaccione Gorge
Gubbio
Quarry fronts
Other sections:
CR - Contessa Road
CQ - Contessa Quarry
CH - Contessa Highway
LEGEND
Bedding
Fault and
Tectonic contact
Sedimentary contact
Quaternary deposits
Marnoso-Arenacea fm (Serravallian-Tortonian)
Schlier fm (Langhian-Serravallian)
Bisciaro fm (Aquitanian-Burdigalian)
Scaglia Cinerea fm (Upper Eocene-Oligocene)
Scaglia Variegata fm (Middle Eocene-Upper Eocene)
Scaglia Rossa fm (Lower Turonian-Middle Eocene)
Scaglia Bianca fm (Upper Albian-Lower Turonian)
Marne a Fucoidi fm (Lower Aptian-Upper Albian)
Maiolica fm (Upper Tithonian-Lower Aptian)
Calcari Diasprigni fm (Callovian-Upper Kimmeridgian)
12°33.7'E
12°33.9'
43°23'N
43°22.7'
CONTESSA MARKER BED
FANO
OSTERIA DI VALDERCHIA
QUARRY FRONT 2001
FAULT
CH
CQ
FAULT
CR
0
100 m
GUBBIO

FIGURE 1

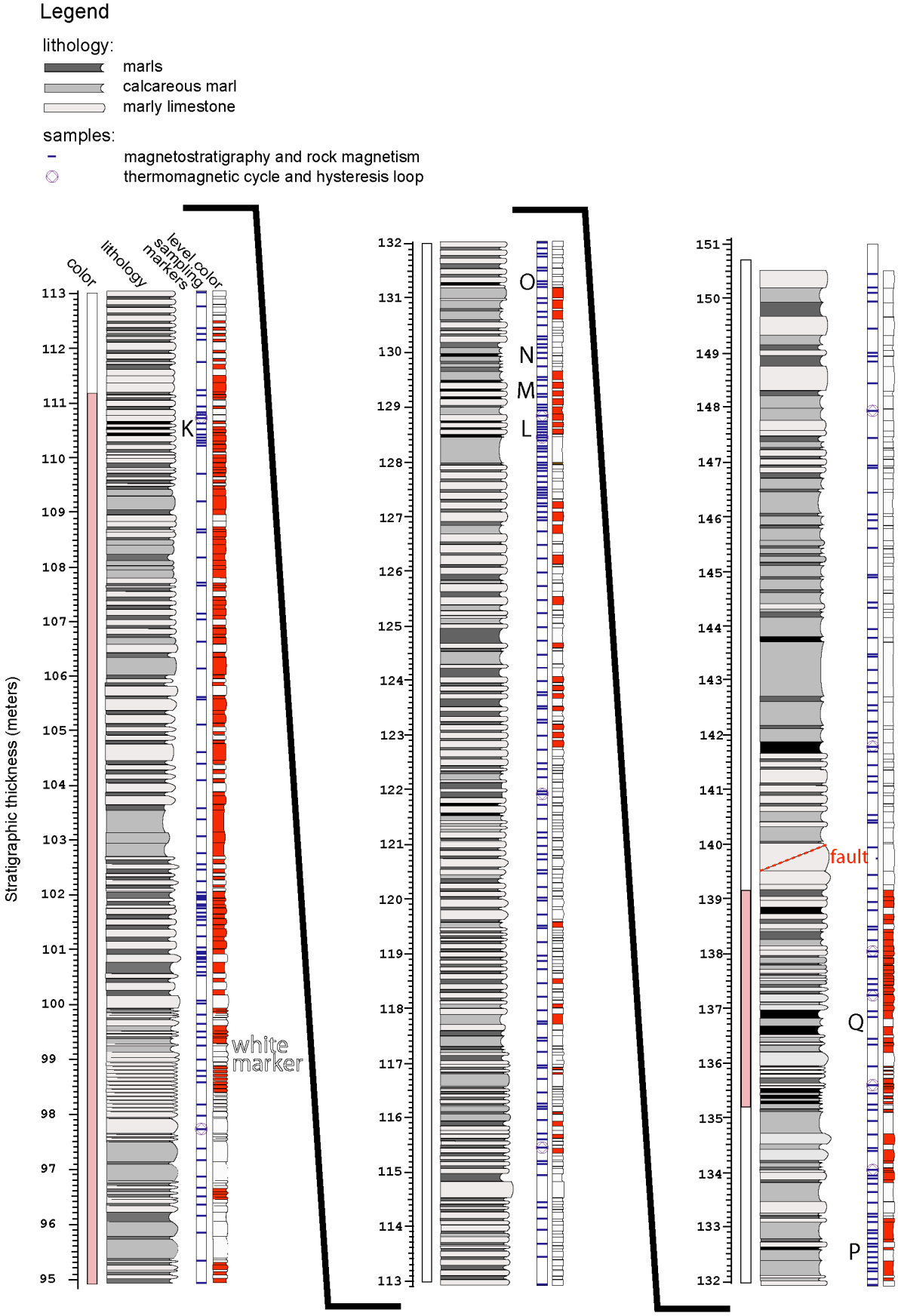
Legend
lithology:
marls
calcareous marl
marly limestone
samples:
magnetostratigraphy and rock magnetism
thermomagnetic cycle and hysteresis loop
Stratigraphic thickness (meters)
color
lithology
level sampling markers
color
K
white marker
O
N
M
L
fault
Q
P

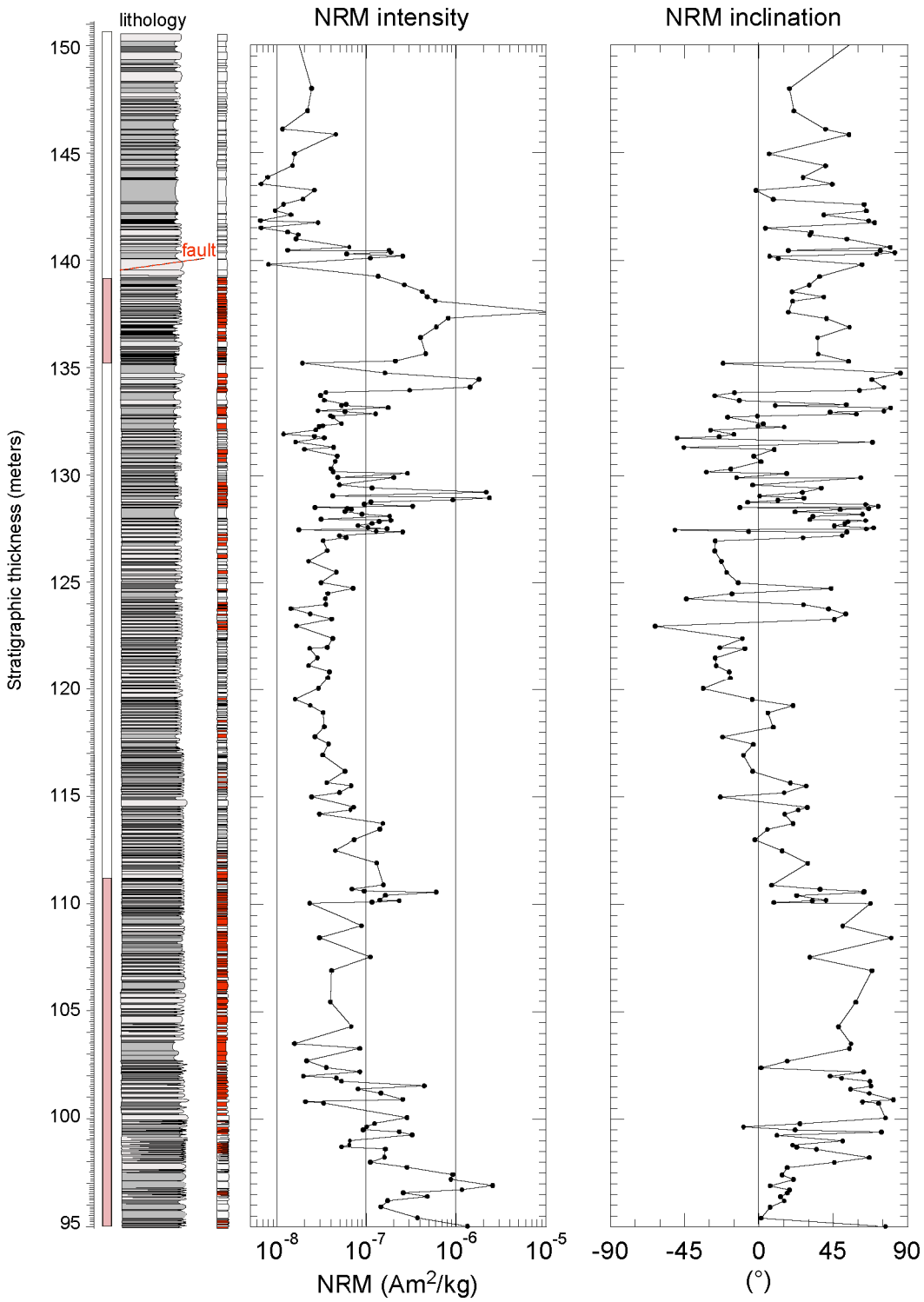
lithology
NRM intensity
NRM inclination
Stratigraphic thickness (meters)
150
145
140
135
130
125
120
115
110
105
100
95
fault
10^{-8}
10^{-7}
10^{-6}
10^{-5}
NRM (Am^2/kg)
-90
-45
0
45
90
(°)

FIGURE 3

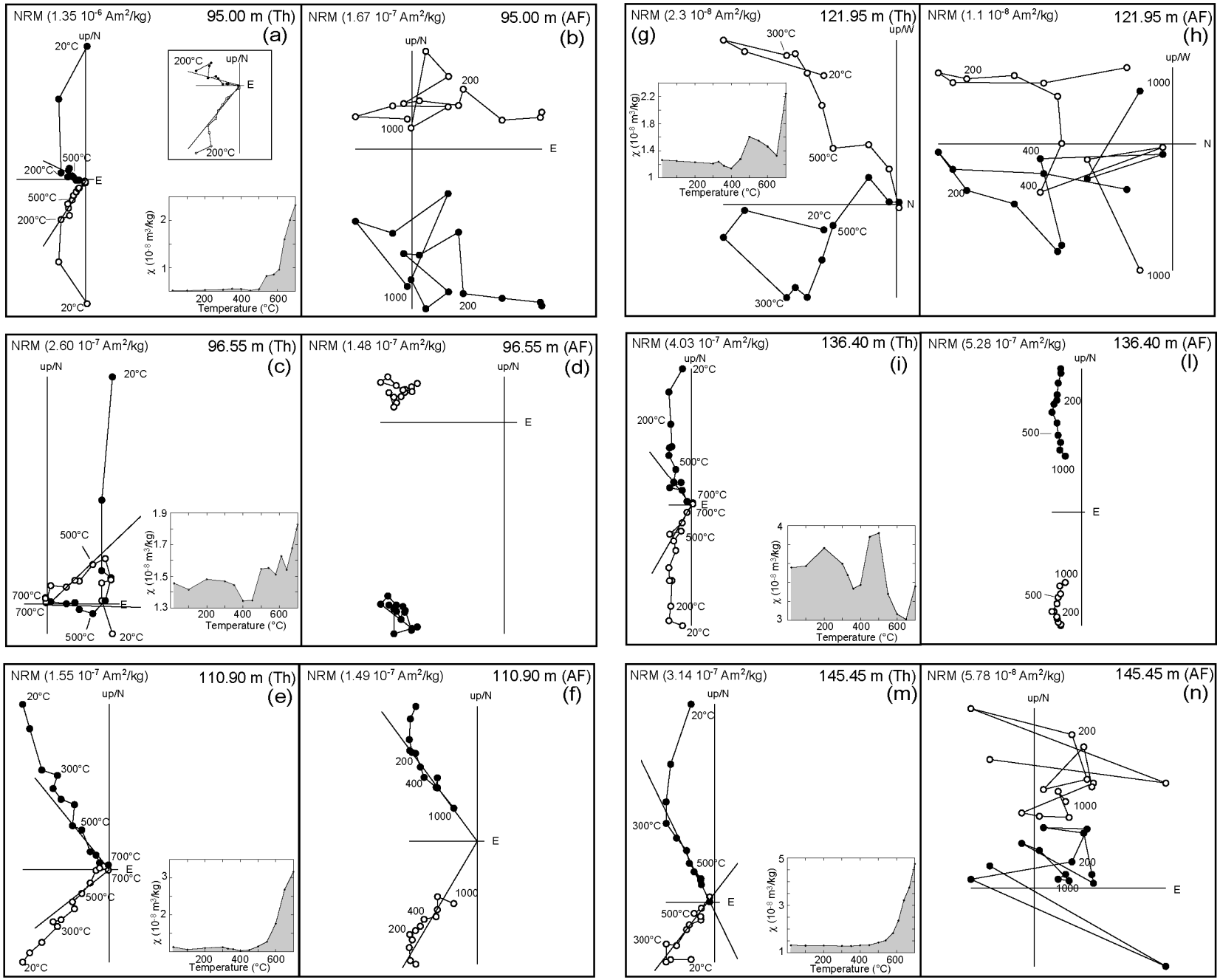
NRM (1.35 10-6 Am2/kg)
95.00 m (Th)
(a)
up/N
20°C
200°C
500°C
E
χ (10-8 m3/kg)
Temperature (°C)
NRM (1.67 10-7 Am2/kg)
95.00 m (AF)
(b)
NRM (2.60 10-7 Am2/kg)
96.55 m (Th)
(c)
700°C
NRM (1.48 10-7 Am2/kg)
96.55 m (AF)
(d)
NRM (1.55 10-7 Am2/kg)
110.90 m (Th)
(e)
300°C
NRM (1.49 10-7 Am2/kg)
110.90 m (AF)
(f)
NRM (2.3 10-8 Am2/kg)
121.95 m (Th)
(g)
up/W
N
NRM (1.1 10-8 Am2/kg)
121.95 m (AF)
(h)
NRM (4.03 10-7 Am2/kg)
136.40 m (Th)
(i)
NRM (5.28 10-7 Am2/kg)
136.40 m (AF)
(l)
NRM (3.14 10-7 Am2/kg)
145.45 m (Th)
(m)
NRM (5.78 10-8 Am2/kg)
145.45 m (AF)
(n)

FIGURE 4

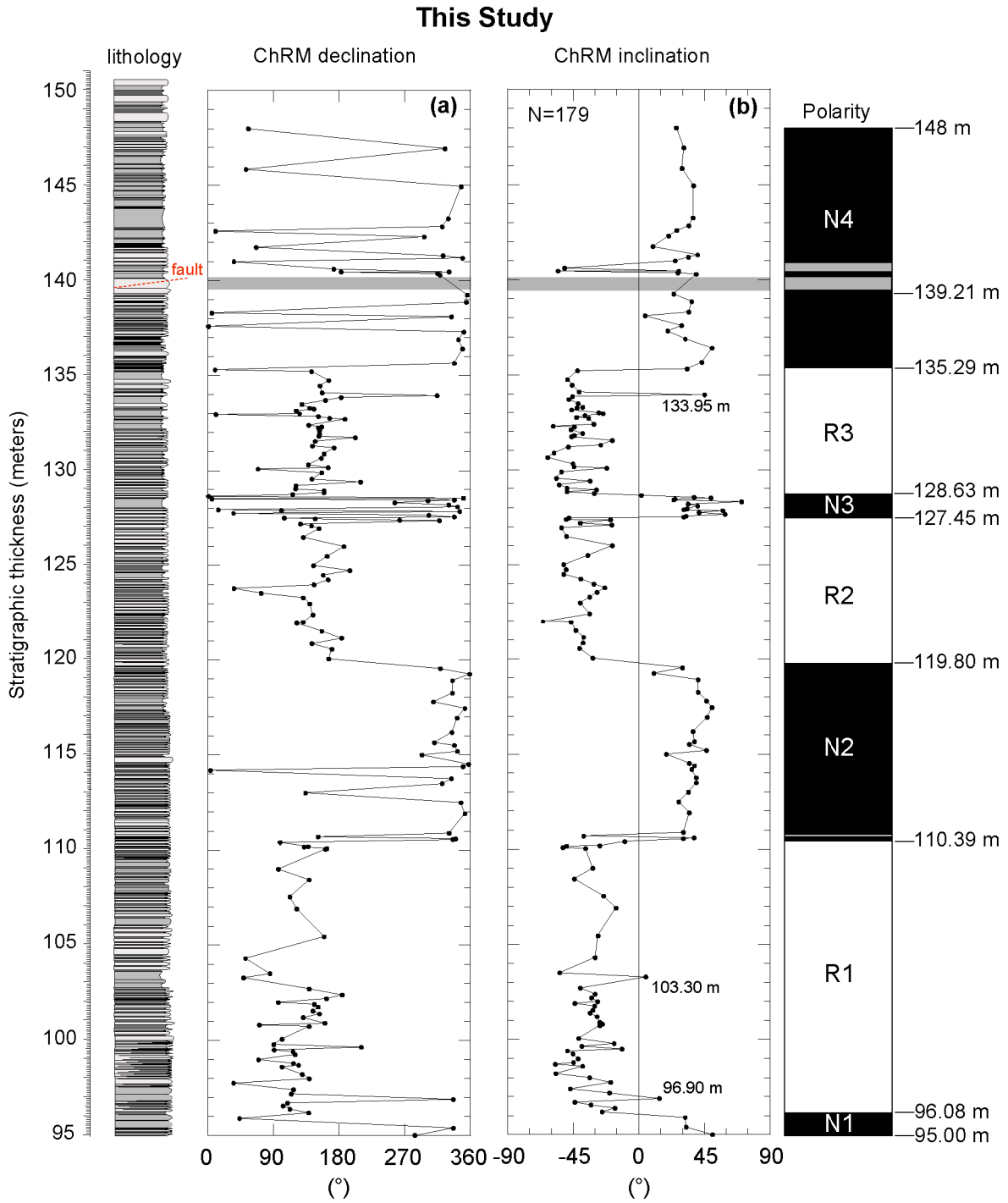
This Study
lithology
ChRM declination
ChRM inclination
(a)
(b)
N=179
Polarity
fault
Stratigraphic thickness (meters)
150
145
140
135
130
125
120
115
110
105
100
95
148 m
139.21 m
135.29 m
128.63 m
127.45 m
119.80 m
110.39 m
96.08 m
95.00 m
N4
R3
N3
R2
N2
R1
N1
133.95 m
103.30 m
96.90 m
0
90
180
270
360
(°)
-90
-45
0
45
90
(°)

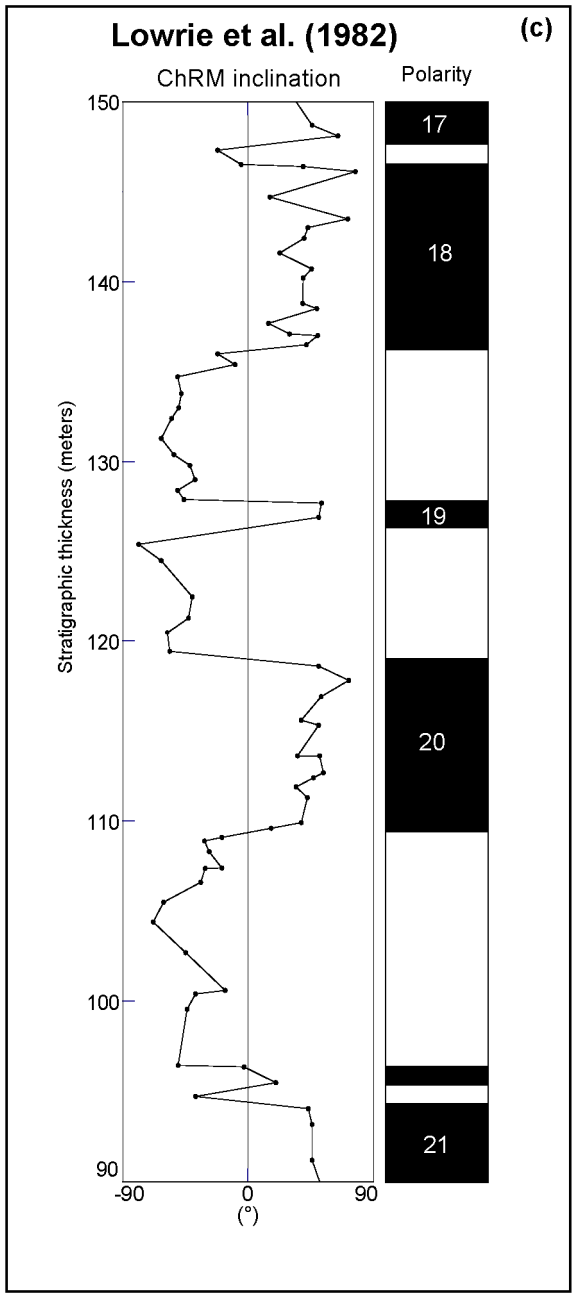
Lowrie et al. (1982)
(c)
ChRM inclination
Polarity
Stratigraphic thickness (meters)
150
140
130
120
110
100
90
17
18
19
20
21
-90
0
90
(°)

FIGURE 5

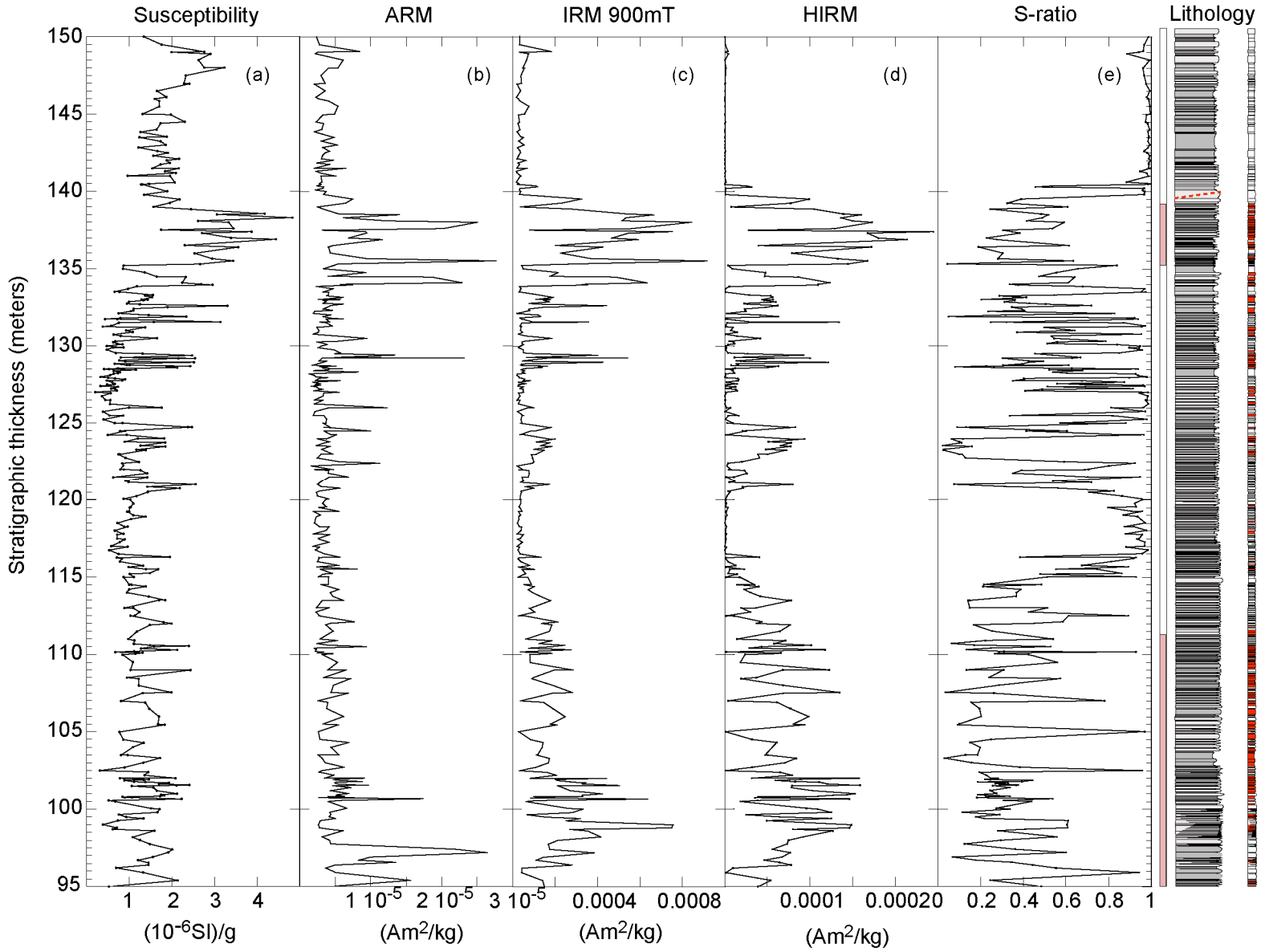
Susceptibility
ARM
IRM 900mT
HIRM
S-ratio
Lithology
(a)
(b)
(c)
(d)
(e)
Stratigraphic thickness (meters)
150
145
140
135
130
125
120
115
110
105
100
95
1
2
3
4
(10-6SI)/g
1 10-5
2 10-5
3 10-5
(Am2/kg)
0.0004
0.0008
(Am2/kg)
0.0001
0.00020
(Am2/kg)
0.2
0.4
0.6
0.8
1

FIGURE 6

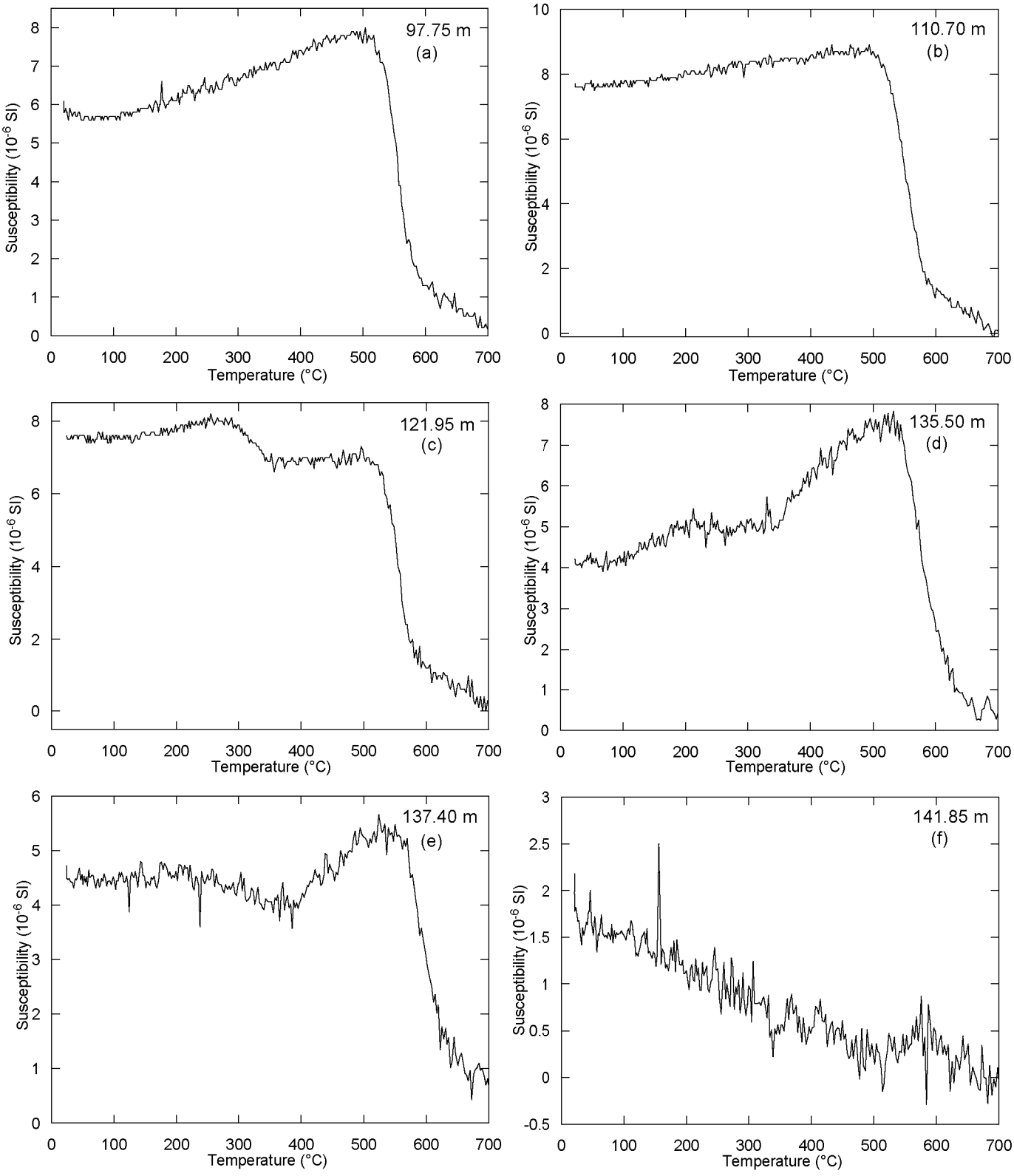
97.75 m
(a)
110.70 m
(b)
121.95 m
(c)
135.50 m
(d)
137.40 m
(e)
141.85 m
(f)
Susceptibility (10-6 SI)
Temperature (°C)

FIGURE 7

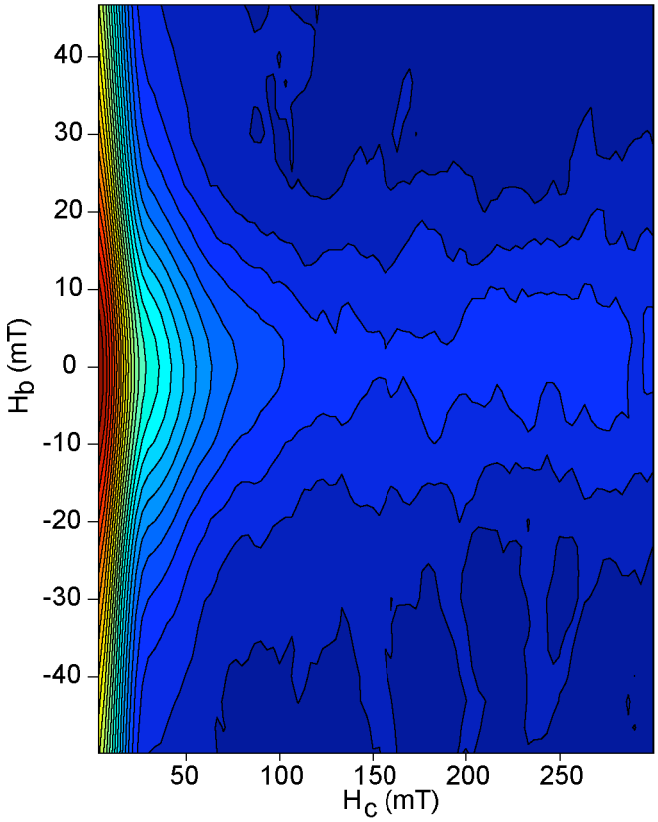

FIGURE 8

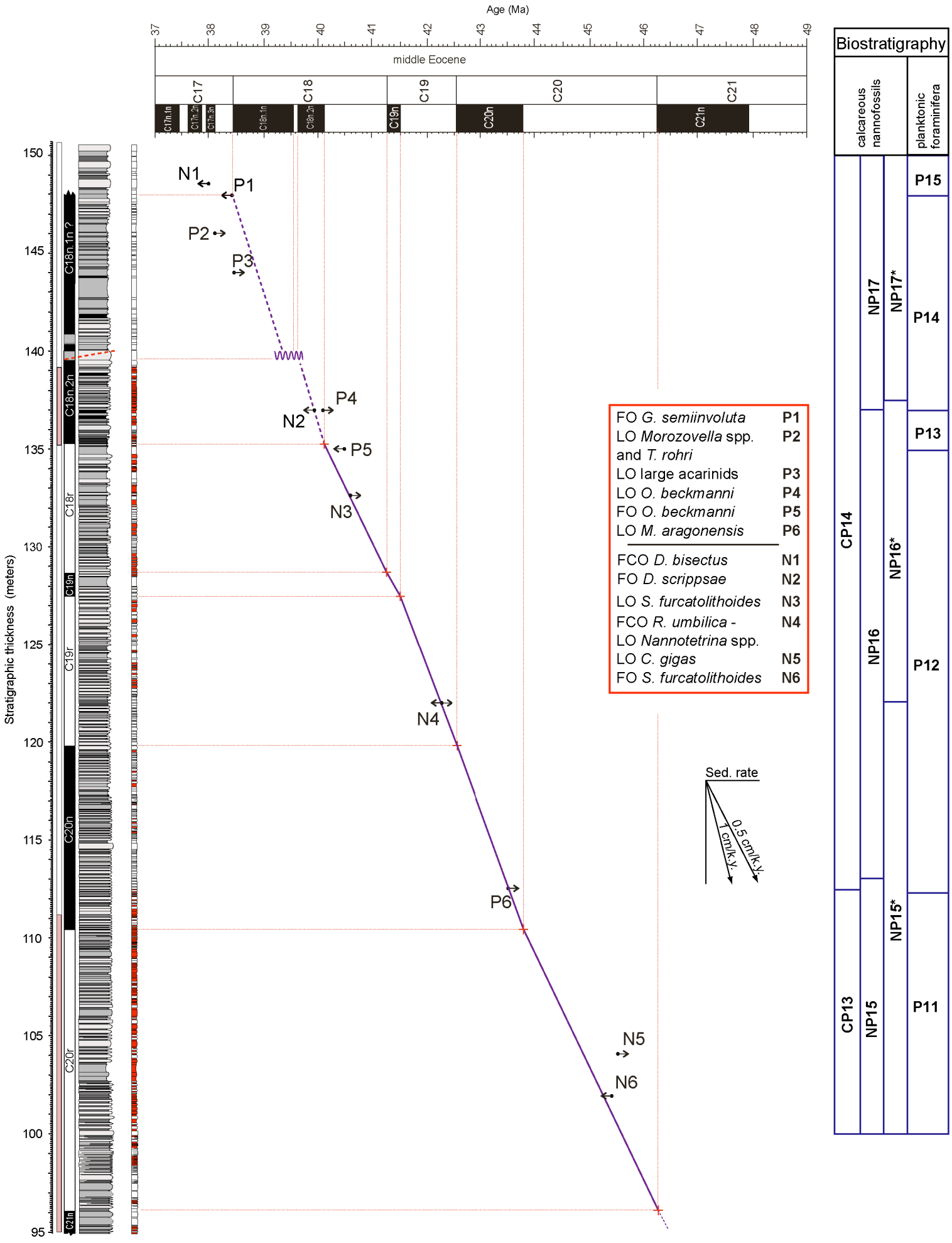
Age (Ma)
middle Eocene
C17
C18
C19
C20
C21
Stratigraphic thickness (meters)
C18n.1n ?
C18n.2n
C18r
C19n
C19r
C20n
C20r
C21n
N1
P1
P2
P3
N2
P4
P5
N3
N4
P6
N5
N6
FO G. semiinvoluta P1
LO Morozovella spp. and T. rohri P2
LO large acarinids P3
LO O. beckmanni P4
FO O. beckmanni P5
LO M. aragonensis P6
FCO D. bisectus N1
FO D. scrippsae N2
LO S. furcatolithoides N3
FCO R. umbilica - LO Nannotetrina spp. N4
LO C. gigas N5
FO S. furcatolithoides N6
Sed. rate
0.5 cm/k.y.
1 cm/k.y.
Biostratigraphy
calcareous nannofossils
planktonic foraminifera
CP14
CP13
NP17
NP16
NP15
NP17*
NP16*
NP15*
P15
P14
P13
P12
P11

FIGURE 9

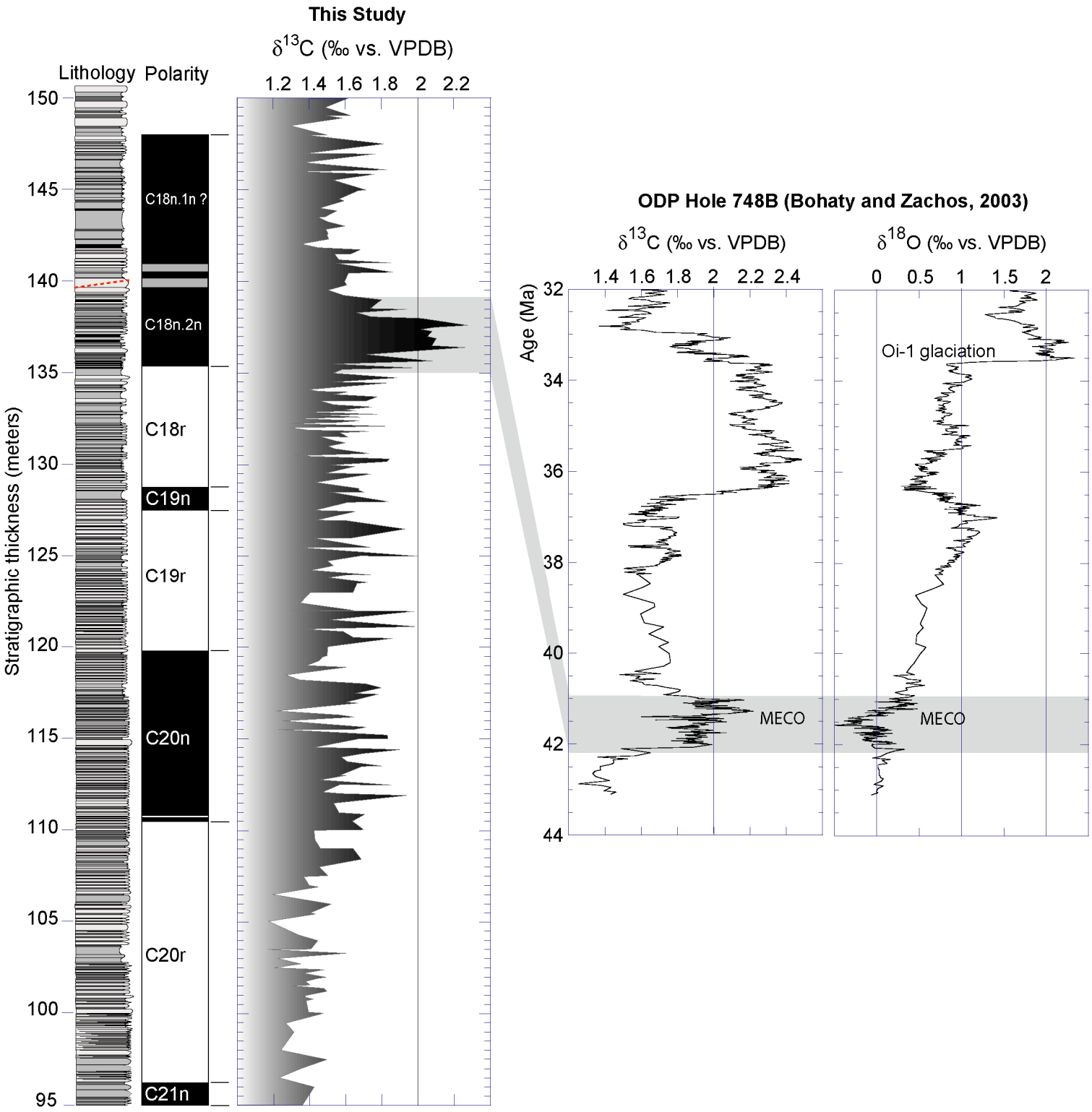
This Study
δ13C (‰ vs. VPDB)
Lithology
Polarity
1.2 1.4 1.6 1.8 2 2.2
150
145
140
135
130
125
120
115
110
105
100
95
Stratigraphic thickness (meters)
C18n.1n ?
C18n.2n
C18r
C19n
C19r
C20n
C20r
C21n
ODP Hole 748B (Bohaty and Zachos, 2003)
δ13C (‰ vs. VPDB)
δ18O (‰ vs. VPDB)
1.4 1.6 1.8 2 2.2 2.4
0 0.5 1 1.5 2
Age (Ma)
32
34
36
38
40
42
44
Oi-1 glaciation
MECO
MECO

FIGURE 10